The Yale Undergraduate Research Journal

Volume 2
Issue 1 *Spring 2021*

Article 37

2021

Strong inclination pacing of climate in Late Triassic low latitudes revealed by the Earth-Saturn tilt cycle

Miranda Margulis-Ohnuma
Yale University

Jessica Whiteside
Yale University

Paul Olsen
Yale University

Follow this and additional works at: https://elischolar.library.yale.edu/yurj

 Part of the Astrophysics and Astronomy Commons, and the Earth Sciences Commons

Recommended Citation

Margulis-Ohnuma, Miranda; Whiteside, Jessica; and Olsen, Paul (2021) "Strong inclination pacing of climate in Late Triassic low latitudes revealed by the Earth-Saturn tilt cycle," *The Yale Undergraduate Research Journal*: Vol. 2 : Iss. 1 , Article 37.
Available at: https://elischolar.library.yale.edu/yurj/vol2/iss1/37

This Article is brought to you for free and open access by EliScholar – A Digital Platform for Scholarly Publishing at Yale. It has been accepted for inclusion in The Yale Undergraduate Research Journal by an authorized editor of EliScholar – A Digital Platform for Scholarly Publishing at Yale. For more information, please contact elischolar@yale.edu.

Strong inclination pacing of climate in Late Triassic low latitudes revealed by the Earth-Saturn tilt cycle

By Miranda Margulis-Ohnuma[1], Jessica H. Whiteside[2], Paul E. Olsen[3]

[1] *Department of Earth and Planetary Sciences, Yale University*

[2] *National Oceanography Centre, University of Southampton, Southampton, United Kingdom*

[3] *Lamont-Doherty Earth Observatory of Columbia University, Palisades, New York, USA*

ABSTRACT

Gravitational interactions among masses in the solar system are recorded in Earth's paleoclimate history because variations in the geometry of Earth's orbit and axial orientation modulate insolation. However, astronomical models are unreliable before ~50 Ma due to the chaotic nature of the solar system and therefore must be constrained using geological observations. Here, we use environmental proxies from paleo-tropical Late Triassic lake deposits of the Newark Rift Basin to identify and tune to previously undescribed strong variations in orbital inclination. Tuning to the 173 kyr Earth-Saturn inclination cycle, theoretically stable due to the high mass of Saturn, reveals both other predicted inclination cycles and previously reported eccentricity cycles. Slight, complementary offsets in the eccentricity and inclination cycles shown by the Earth-Saturn (s3-s6) and Venus-Jupiter (g2-g5) tunings may be due to chaotic variations of the secular fundamental frequencies in Earth's nodal and Venus's perihelion orbital precessions. The strength of the inclination cycles suggests that the Earth system modulates orbital pacing of climate and provides a mechanism to further constrain astronomical solutions for solar system dynamics beyond the ~50 Ma limit of predictability.

INTRODUCTION

The solar system is chaotic, and over long timescales small differences in the initial conditions of numerical models of solar system dynamics lead to vastly different outcomes that are difficult or impossible to predict using calculated solutions (Laskar, 1999) prior to 50 Myr before the present (Hinnov, 2018). But the gravitational interactions of the sun, planets, moons, and other masses produce climate changes through deformations of Earth's orbit and axial orientation that are recorded in the geological record, allowing the actual history of these gravitational interactions to be recovered. For example, carbon isotope excursions in the marine carbon cycle of the Late Triassic to Early Jurassic are paced by long-eccentricity cycles (Storm et al., 2020). Environmental changes of orbital origin also influence patterns of evolution and extinction (Li et al., 2016), such as those of Late Triassic fish (Whiteside et al., 2011b), and influence speciation by sorting species into distinct provinces (Whiteside et al., 2011a). The most famous example of orbital pacing of climate is the Pleistocene Ice Ages, paced by orbital eccentricity, precession, and obliquity of Earth's axis (Hays et al., 1976).

The Newark Basin, currently in eastern North America, was located in the tropics to subtropics during the Triassic and Early Jurassic. Sequences in this region from 201–221 Ma represent a low-latitude record of the Late Triassic, a period with no ice sheets, testing CO_2 control of hydrology. In particular, very low CO_2 levels likely caused muted cyclicity in the top of the section, potentially allowing evidence of inclination control of climate to appear more easily. The Newark Basin Coring Project (NBCP) data consists of proxies of lake depth, which itself can be used as a climate proxy: astronomical cycles drive variations in solar insolation and hence paleoclimate trends. The lake depth proxies consist of sedimentary structures and fabrics, color, natural gamma radioactivity, and sonic velocity (Olsen & Kent, 1996), but geochemical data or any other measurable features that vary with lake depth could be used. Olsen et al. (2019) used Late Triassic cores of lake sediments from the NBCP and Colorado Plateau Coring Project (CPCP) to calculate the values of the secular precession of perihelion (the change in the point on a planet's orbit closest to the sun as the shape of the orbit changes) of the inner planets (g values, g1, g2, g3, g4), and to demonstrate that the Earth-Mars eccentricity cycle (g3-g4; the

Named lithological expression of cycles	Description	Argument	Periods and informal names of Milankovitch or orbital cycle with today's period
Van Houten cycle	Precession frequency of Earth (p) + secular frequency of precession of perihelion of Mercury, Venus...	p + g1, p + g2, p + g3, p + g4, p + g5	~21 kyr (average 21.5 kyr); 23.2-, 22.4-, 19.2-, 19.0-, 23.8-kyr climatic precession
Short modulating cycle	Secular frequencies of precession of perihelion of Mars – that of Jupiter, etc.	g4 - g5, g2 - g3, g2 - g4, g2 - g3	~100 kyr (average 112.1 kyr); 94.9-, 98.9-, 123.9-, 130.7-kyr short obliquity
McLaughlin cycle	Venus (g2) – Jupiter (g5)	g2 - g5	405-kyr long orbital eccentricity Grand Cycle
Long modulating cycle	Earth (g3) – Mars (g4)	g3 - g4	2,365-kyr Grand Cycle

Table 1. *Important cycles reflecting orbital eccentricity and axial precession, modified from Olsen et al. (2019).*

Published by EliScholar – A Digital Platform for Scholarly Publishing at Yale, 2021

difference between the precession of perihelion cycles of Earth and Mars) during the Late Triassic had a period of 1.8 Myr as opposed to the modern value of 2.4 Myr. This geological data allowed the La2010d solution (Laskar et al., 2011) to be identified as the best of four current representations of solar system evolution for the Late Triassic, as opposed to La2010a (Laskar et al., 2011), the favored solution for the present (Olsen et al., 2019).

In all analyses of astronomical influences on climate as recorded in geological records, there is at least some variation in accumulation rate (Muller & Macdonald, 2000). Since thickness is the first order proxy for time, accumulation rate changes must be accounted for prior to time series analysis and recovery of the values for astronomical parameters. Ideally, this would be done by densely spaced radioisotopic dates, but because that requires the presence of datable, usually igneous, minerals, "tuning" by fitting the data to numerically constant, known astronomical cycles is more frequently used. "Minimal tuning," the process of tuning to the smallest possible number of parameters, is critical in reducing tuning biases; the success of the tuning depends on the expression of other astronomical terms than the one tuned to, with the best tuning causing a significant increase in the power of independent frequencies (Muller & MacDonald, 2000). The cycle most commonly used for tuning in Mesozoic strata is the 405 kyr Venus-Jupiter (g2-g5) "long" eccentricity cycle (Hinnov, 2018), the most prominent and stable term in the eccentricity solution (Laskar et al., 2011). This frequency is a difference cycle of the secular fundamental frequencies of perihelion precession of Venus and Jupiter, g2-g5. It is considered an astronomical "metronome," meaning it is very stable over long time scales because the large mass of Jupiter results in a g5 variability of only 0.0007% (Laskar et al., 2004).

Additionally, independent calibration of the NBCP record is provided by zircon U-Pb CA-ID-TIMS ages (Blackburn et al., 2013) on lava flows interbedded with lacustrine strata overlying the upper Passaic Formation combined with ages from older strata from the CPCP, correlated to the NBCP sequence by paleomagnetic polarity stratigraphy. This correlation confirms the validity of the astrochronostratigraphic polarity time scale (APTS), which is based on a theoretically stable 405 kyr cycle, thus validating the theoretical known stability of the cycle (Kent et al., 2018; Olsen et al., 2019; Rasmussen et al., 2020).

A similar but less familiar metronome, the 173 kyr Earth-Saturn inclination cycle (s3-s6), where the "s" frequencies reflect the precession of the nodes of the planetary orbits, was shown using astronomical solutions to be stable up to 50 Ma and used to tune middle Eocene sequences, closing the "Eocene astronomical timescale gap" (Boulila et al., 2018). In this study, we identify the s3-s6 cycle in a subset of the Newark Basin section and use astronomical solutions to show the stability of this cycle into the Late Triassic. By successfully tuning to the 173 kyr inclination cycle and re-tuning to the 405 kyr eccentricity cycle using an age model based on gamma ray data as a proxy of lake depth, climate, and ultimately gravitational interactions within the solar system, we present an interval in which a more accurate tuning can be calculated independent of the chaotic drift of Venus and Earth.

METHODS

Time Series Analysis

We began by dividing the Newark data into four intervals of equal length (5.1 Myr), informed by the qualitative differences in the character of the data in Intervals I and IV as well as lithological differences (Figure 1). Three different proxies of lake depth were used to study the potential role of orbital cyclicity in this interval: depth rank from the core, a subjective value on a scale of 0–5 based on lithology that represents lacustrine depth at the time of deposition (Olsen & Kent, 1996), natural gamma radioactivity, and sonic velocity from the borehole, which reflects differences in rock composition based on the speed of sonic waves through the section. Gamma and sonic data were clipped at the mean of each dataset to reduce potential destructive interference of symmetrical portions of the curve, and the upper and lower halves of each dataset were analyzed separately. We analyzed each proxy in each interval using the multi-taper method (MTM) spectral analysis in Acycle, a MATLAB program for time series analysis (Li et al., 2019). MTM analysis, first presented by Thomson (1982), uses windowed trials to assess each data point multiple times, and is therefore more accurate, if less precise than the conventional fast Fourier transform; it reduces spectral leakage compared to single taper analysis (Park et al., 1987). Additionally, we used f-significance peaks generated by Acycle to determine the most representative cycles in our data. We used power spectra to provide a visual representation of results from the entire data interval with the assumption the data are stationary in frequency, and evolutionary spectral analysis to provide

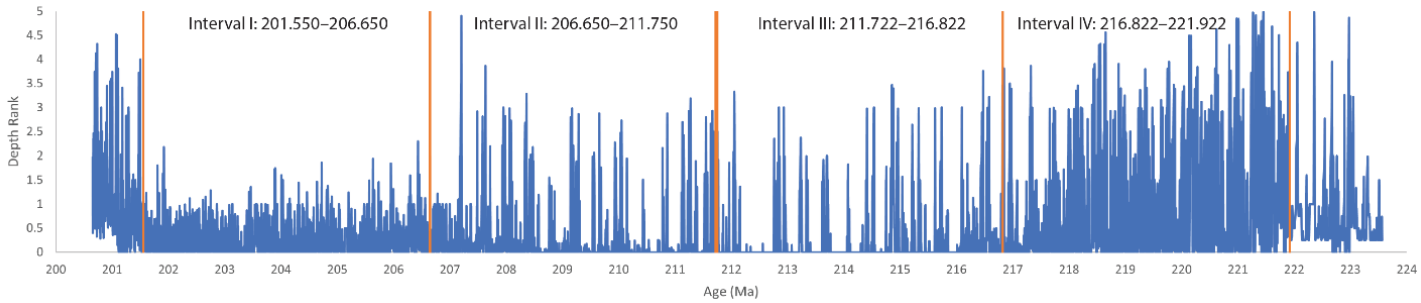

Figure 1. *The four 5.1 Myr intervals of the depth rank data (value on a scale of 0–5). Interval I is characterized by dense, low amplitude data and red mudstone; Interval IV by dense, high amplitude data. Note the small overlap between Intervals II and III to ensure a consistent length of each interval. The very top and bottom of the sequence are excluded due to their qualitative difference and short duration compared to the intervals.*

a visual representation of our results as they evolved through time without an assumption of stationarity.

Astronomical Solutions

Olsen et al. (2019) compared the Newark sequence to the La2004 eccentricity and clipped obliquity astronomical solutions of Laskar et al. (2004) individually before concluding that the La2010d Triassic solution most closely resembles the data over this interval. Therefore, we used the La2010d solution and the La2010a solution, which is favored for the present, as references for our spectra. We combined the eccentricity and clipped obliquity for each solution by adding and normalizing them such that our final solutions consisted of equal parts eccentricity and obliquity. An amplitude modulation was performed in Acycle to remove the 40 kyr precession cycle so the solutions represented orbital inclination instead of true obliquity. Other methods used to combine eccentricity and obliquity, the insolation equation and eccentricity-tilt-precession (ETP) models, do not show obliquity as much as these new versions of the solutions do; our solutions do not represent a natural phenomenon but instead a frame of reference for both eccentricity and obliquity signals.

"The solar system is chaotic, and over long timescales small differences in the initial conditions of numerical models of solar system dynamics lead to **vastly different outcomes**"

Numerical Forward and Inverse Experiments

Effect of the small fault in Interval I:
Variations in sedimentation rate can cause split peaks in power spectra, where the power originally at one peak is distributed among several frequencies (Muller & Macdonald, 2000). There is a fault in the sequence at 203.249 Ma (in Interval I) that we know little about geologically, but that may have caused a duplication or elimination of some of the section. To investigate whether the fault might also cause peak splitting, we conducted a series of forward experiments, first with a simple sine wave, then with the modern La2010a solution. We began with a pure sinusoid with a period of 100 kyr over 600 kyr, from which we removed 50 kyr in the middle. As a sensitivity test, we repeated this process over a 5 Myr interval, again removing 50 kyr. Both of these preliminary experiments showed peak splitting as predicted. We then repeated the experiment with the modern La2010a solutions for eccentricity and clipped obliquity. To induce the largest possible offset, we removed 202 kyr from the eccentricity solution and 86 kyr from the obliquity solution, about one half of their respective prominent cycles. These forward experiments also showed evidence of peak splitting (see Results).

Theoretical Stability of the g3-g6 Earth-Saturn Cycle:
In order to be used as a metronome, a cycle must not be significantly affected by chaotic drift over the relevant time period. While the 173 kyr cycle is predicted to be stable due to the large mass of Saturn, this has only been shown up to 50 Ma (Boulila et al., 2018), with stability further back than that never previously investigated. We used the La2010a, La2010b, La2010c, and La2010d obliquity solutions for the present (0–20 Ma) and for the Triassic (201–221 Ma) to model the effect of chaos on this cycle under different initial conditions, testing the stability of the cycle through the Late Triassic, and confirmed that it can be used as a metronome (see Results).

Tuning to the 173 kyr and 405 kyr cycles

All tuning was performed using the "Age Scale | Tuning" function in Acycle. High power peaks in the FFT of the raw data representing each cycle were identified as centers and appropriate bandwidths were chosen using the "Filtering" option. To tune to the s3-s6 cycle, we used a center of 0.010526 cycles/ft. and a filter bandwidth of 0.0048 cycles/ft.; for the g2-g5 cycle, we used a center of 0.016917 cycles/ft. and a bandwidth of 0.01 cycles/ft. Age models were created based on gamma ray data using the "Build Age Model" function, with the periods entered as "173" and "405" respectively. This generates the input for the "Age Model" section of the "Age Scale | Tuning" function, with the raw data for each proxy input into the "Series" section. We then interpolated the data using the Acycle "Interpolation" function to ensure an evenly spaced dataset for MTM spectral analysis, using the median of each dataset as the new sample rate. The "TimeOpt" function was used to assess the objectivity of the sedimentation rate. For comparison, we cut each dataset to the same length, interpolated to 0.001 Myr, ran spectral analyses, and re-interpolated the results to 0.0588 Myr, the approximate sample rate of each dataset after spectral analysis.

RESULTS

Upper Passaic Formation

Our initial analyses of the four segments, MTM power spectra at both 3π and 4π bandwidths, suggested that the behavior of Interval I, in the upper Passaic Formation, showed fundamental differences compared to the other intervals. First, as we knew, the amplitude of variations of all proxies was lower (e.g. Figure 1). Second, based on the time constraints provided by U-Pb ages, spectral analysis of the untuned interval revealed strong f-significance peaks in the short-eccentricity range but lower power in the 405 kyr (g2-g5) range, unlike the rest of the record. In Intervals II, III, and IV, peak agreement between proxies was less clear in the short eccentricity range. Although the 405 kyr cycle came through strongly in each interval, the Interval II gamma ray 405 kyr peak was split. Intervals II, III, and IV also had high power in the short eccentricity range and low power in the obliquity range. Most significantly, in Interval I, spectral peaks ~170–175 kyr and ~1.4 Myr in the untuned data, again constrained by the U-Pb ages, suggested unusually strong inclination pacing in this interval. Therefore, we focused our additional experimentation and analysis on Interval 1.

Published by EliScholar – A Digital Platform for Scholarly Publishing at Yale, 2021

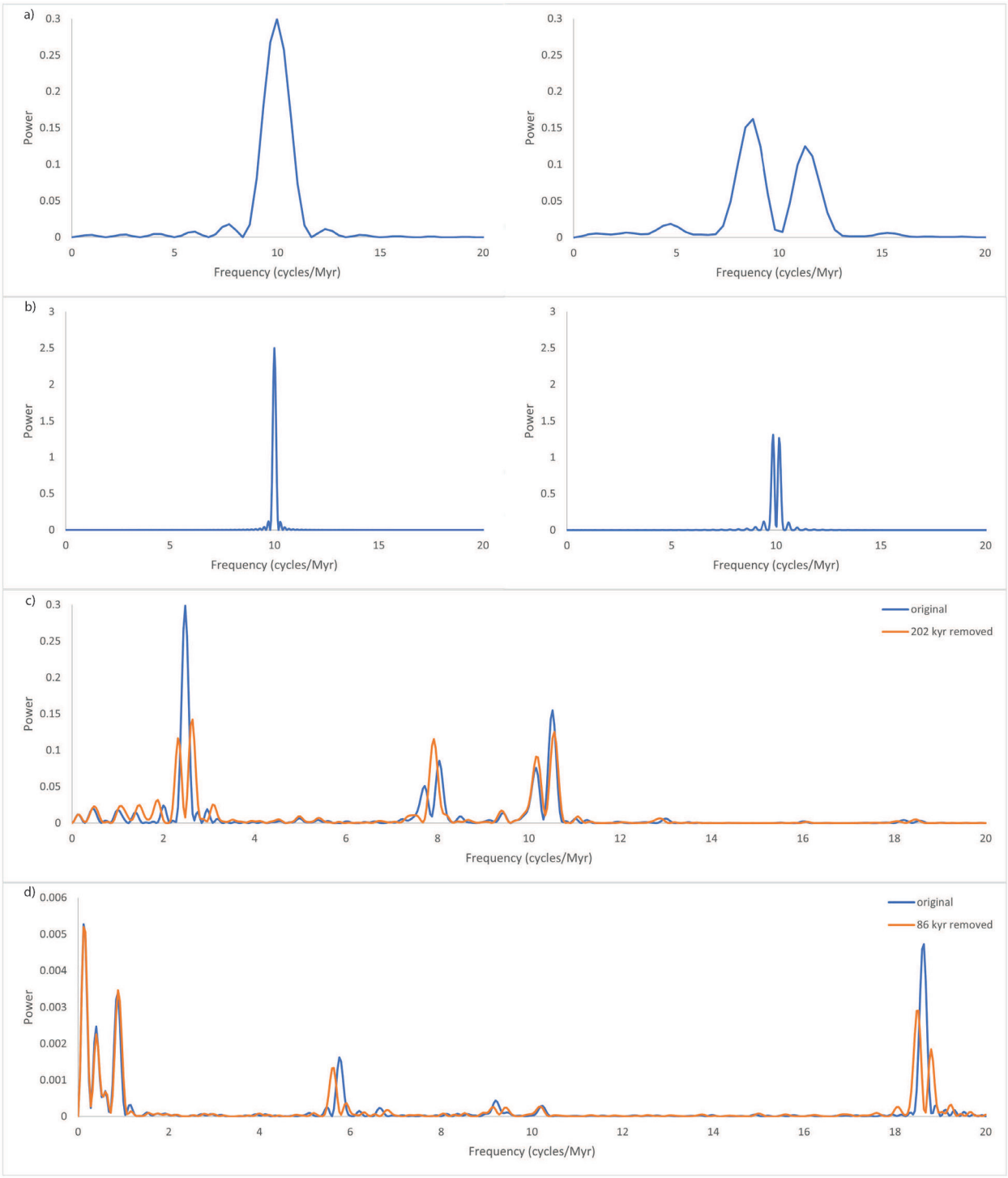

Figure 2. *Results from forward experiments to investigate peak splitting. a) periodogram of a 600 kyr long section of a sine wave with a 100 kyr period, before and after 50 kyr removed, b) periodogram of a 5 Myr long section of a sine wave with a 100 kyr period, before and after 50 kyr removed, c) periodogram of the La2010a eccentricity solution from 0–5 Ma, before and after 202 kyr removed, d) periodogram of the La2010a obliquity solution from 0–5 Ma, before and after 86 kyr removed. Peak splitting occurs ~2.5 cycles/Myr in the eccentricity solution and ~9 and ~18 cycles/Myr in the obliquity solution.*

Numerical Forward and Inverse Experiments

Effect of the small fault in Interval I:

Each of our forward experiments to model the potential effect of the fault in our section resulted in peak splitting. The first experiment, in which a 50 kyr segment was removed from a sine wave with a period of 100 kyr over 600 kyr, resulted in two peaks on either side of the original peak (Figure 2a). The sensitivity test over 5 Myr (the approximate length of each of our intervals) showed a split peak as well, although the frequency of each of the new peaks was closer to the frequency of the original peak than in the first experiment (Figure 2b). In the La2010a solution for the present, some peak splitting occurred in both the eccentricity and obliquity models (Figure 2c, d). To minimize the effect on our results, we restricted further analysis to the portion of Interval I below the fault, from 203.249–206.650 Ma.

Theoretical Stability of the g3-g6 Earth-Saturn Cycle:
Spectral analysis showed that a peak ranging from 170.657–175.140 kyr was clearly prominent and highly significant (f value <0.025) in each of the La2010 obliquity solutions (Figure 3). As a control, each of the solutions was also analyzed for the present, and each showed a prominent and highly significant peak at 172.720 kyr. Thus, chaotic drift could have only a small effect on this peak back to the Late Triassic. This is consistent with our expectations due to the large mass of Saturn; like the precession of perihelion of Jupiter's orbit (g5) (Kent et al., 2018), the precession of the nodes of Saturn's orbit (s6) is stable over long timescales.

Time Series Analysis

All three proxies in Interval I (below the fault) yielded similar spectrum shapes and f-significant peaks (Figure 4), indicating that the original tuning to the 405 kyr g2-g5 cycle using a depth rank age model was appropriate, if not ideal. Clipping the gamma ray and sonic velocity data at their respective means showed similar spectra for the upper half, lower half, and unclipped datasets, indicating insignificant destructive interference; consequently, we used the

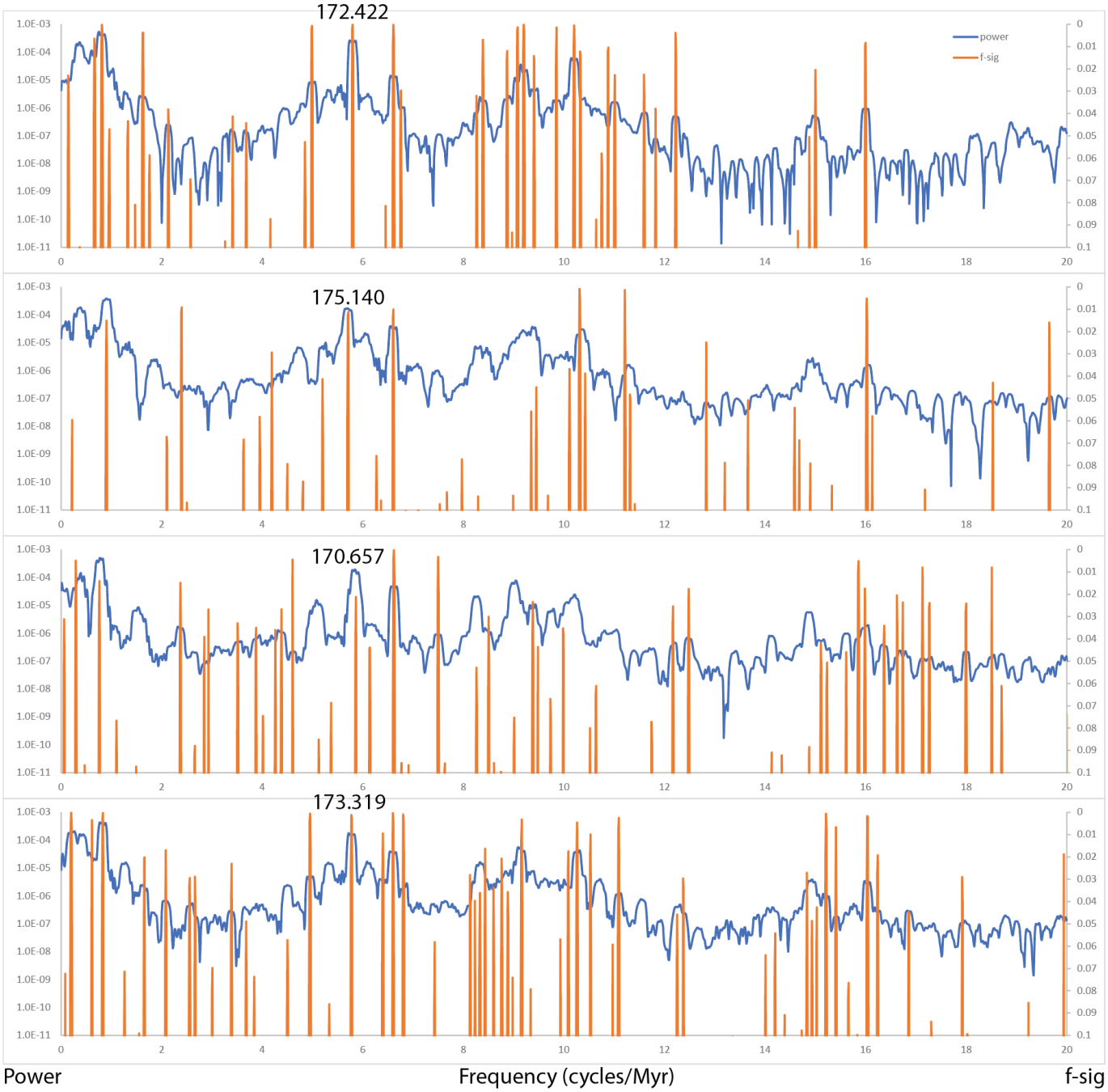

Figure 3. *Stability of the 173 kyr cycle using astronomical solutions, plotted on a logarithmic scale. MTM power spectra with 2π bandwidth of, from top to bottom: La2010a, La2010b, La2010c, and La2010d obliquity solutions for 201–221 Ma. The f-significance value peak ~173 is clearly present in all solutions, but differs slightly due to Earth's chaotic drift and modulation by longer frequency cycles.*

Published by EliScholar – A Digital Platform for Scholarly Publishing at Yale, 2021

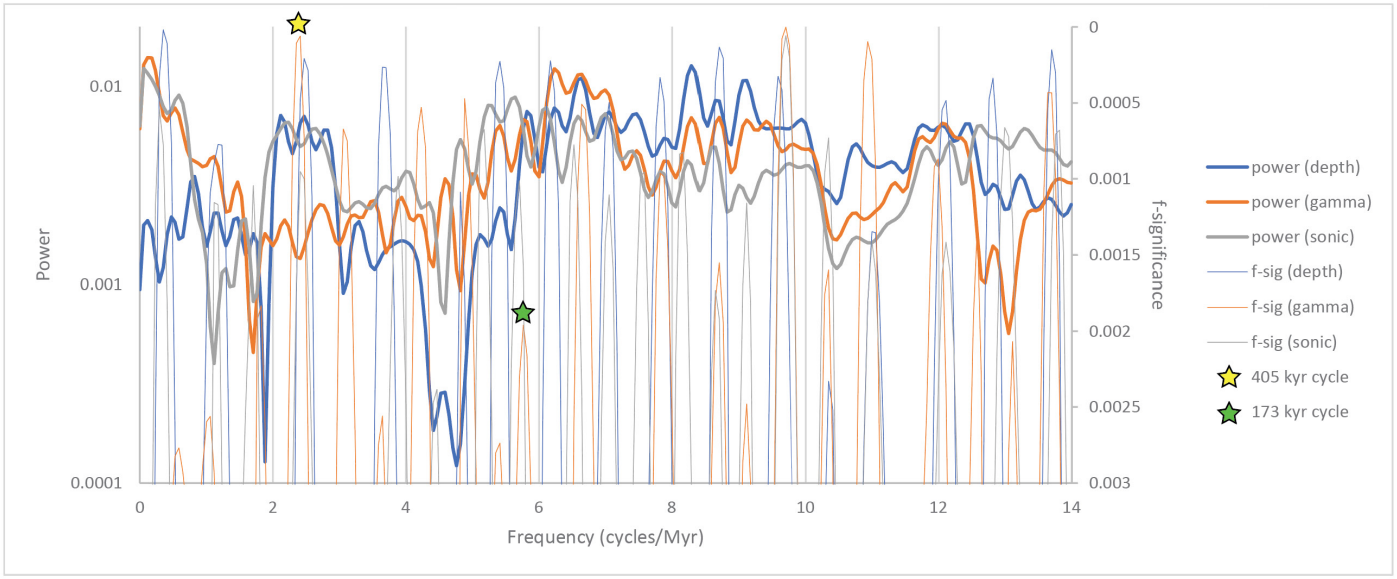

Figure 4. *MTM power spectra of three proxies (depth rank, gamma ray, sonic velocity) on a logarithmic scale and corresponding f-significance values of Interval I below the fault (203.249–206.650 Ma), with original tuning to the 405 kyr cycle based on a depth rank age model, at a 2π bandwidth. The 405 kyr cycle is shown in all three proxies at the peak ~2.5, and the short eccentricity cycles appear as overlapping peaks at ~10 cycles/Myr.*

unclipped data. A conspicuous high-power frequency of 6 cycles per million years in Interval I was identified as the 173 kyr s3-s6 cycle. This is the first evidence of an inclination signal in any part of the Newark sequence.

Tuning to the 173 kyr and 405 kyr cycles

To evaluate the presence and significance of the s3-s6 cycle, we used it as a metronome. After tuning to the 173 kyr cycle, the 405 kyr cycle is clearly visible in the gamma and sonic datasets and, though less significant, can be identified in the depth rank data as well (Figure 5). The new tuning is quite successful, closely matching the overall spectrum shape and significant peaks of the La2010d solution (Figure 6). For the untuned data, both TimeOpt and a manual analysis of the most prominent gamma peak yielded an accumulation rate of 0.48 ft/kyr. The accumulation rate of our new tuned data is 0.44 ft/kyr.

We then re-tuned the raw data to the more commonly used g2-g5 cycle. The result is a spectrum that clearly shows the 173 kyr cycle as well as other prominent eccentricity and obliquity peaks (Figure 6). This new spectrum matches the La2010d solution better than the original tuning to the 405 kyr cycle (Figure 4), which was based on a depth rank age model. Other predicted inclination cycles (s) and previously observed eccentricity cycles (g) are identified and shown in Table 2.

Olsen et al. (2019) used the matrix method as an internal consistency check, in which low frequency cycles are calculated from high frequency cycles, then compared to the observed frequencies (for example, the period of the Venus-Mars inclination cycle, s2-s4, can be calculated from the periods of the Venus-Earth and Earth-Mars cycles, s2-s3 and s3-s4 respectively). We used this method to check our results, not just for eccentricity as in the 2019 paper, but for

Row	Argument	MTM period (kyr) in 173 kyr tuning	MTM period (kyr) in 405 kyr tuning	La2010d period (kyr)	Theoretical Value*
1	s3-s4	1546.07	–	1308.22	1183.34
2	g2-g5	386.52	404.92	404.92	405.69
3	s2-s8	200.08	200.08	204.90	203.83
4	s3-s6	173.54	177.15	173.54	172.85
5	s4-s6	150.5	154.61	151.85	150.82
6	g2-g3	134.98	130.82	133.91	130.70
7	s2-s4	122.35	120.62	123.24	121
8	s2-s3	110.43	111.16	110.43	109.83
9	g3-g5	98.31	–	100.63	98.85
10	g4-g5	–	94.48	94.48	94.89
11	s4-s8	75.59	75.59	76.95	75.95
12	s2-s6	68.3	66.43	67.22	67.16

*calculated from s and g values in Table 4.1 of Laskar (2020)
– no peak present

Table 2. *Identified cycles and their periods shown in the 173 kyr tuning and 405 kyr tuning of the gamma ray data compared to the La2010d solution and theoretical values calculated from Laskar (2020).*

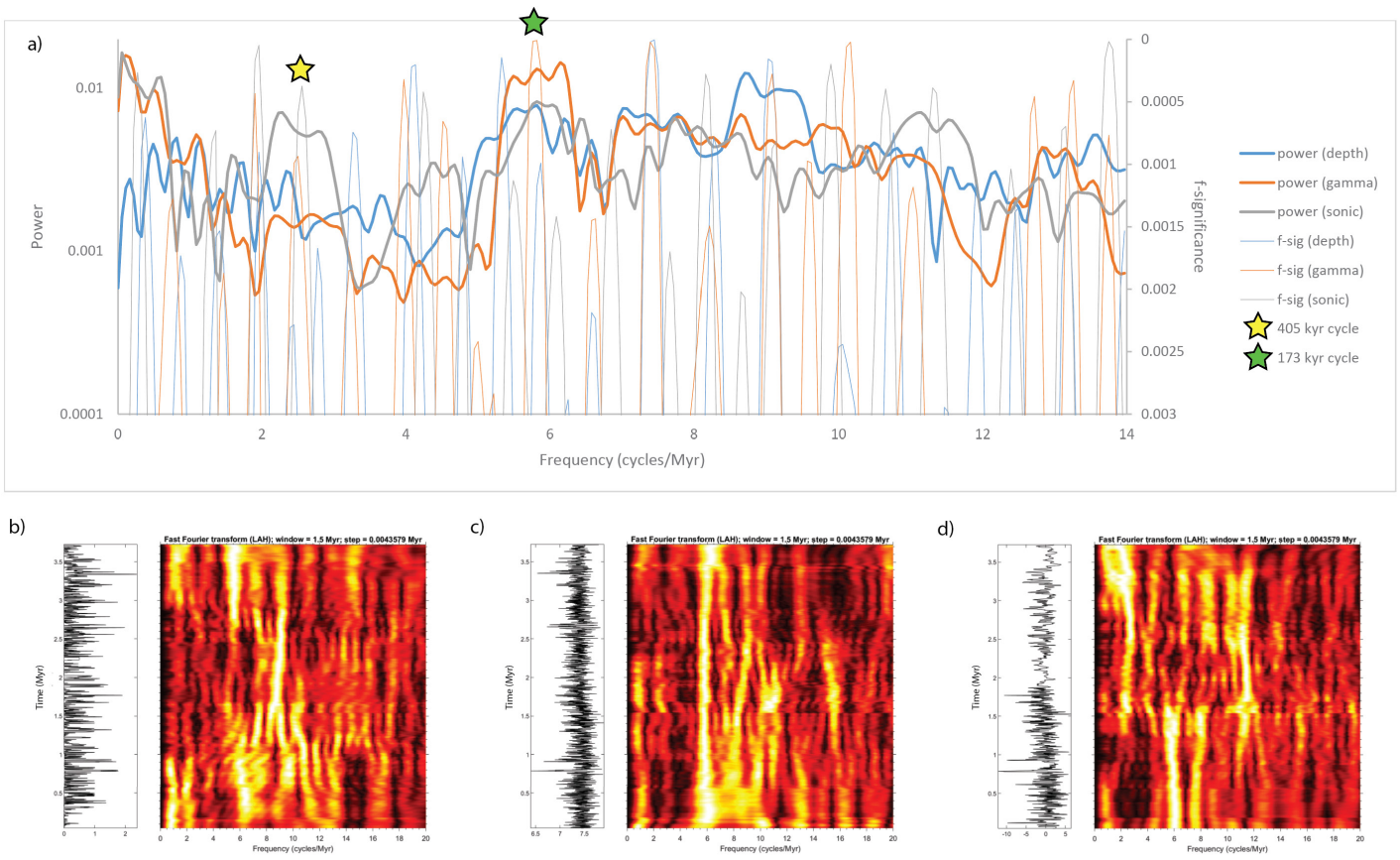

Figure 5. *Results of tuning to the 173 kyr cycle using an age model based on gamma ray data. a) MTM power spectra at 2π bandwidth of three proxies (depth rank, gamma ray, sonic velocity) plotted on a logarithmic scale and corresponding f-significance values of Interval I below the fault. The 405 kyr cycle comes through clearly in the gamma and sonic peaks ~2.5 cycles/Myr, and less clearly in the depth rank peak just to the right. Evolutionary power spectra of b) depth rank, c) gamma ray, and d) sonic velocity. The 405 kyr cycle, 173 kyr cycle, and cycles in the 100 kyr range can be seen as high-power areas.*

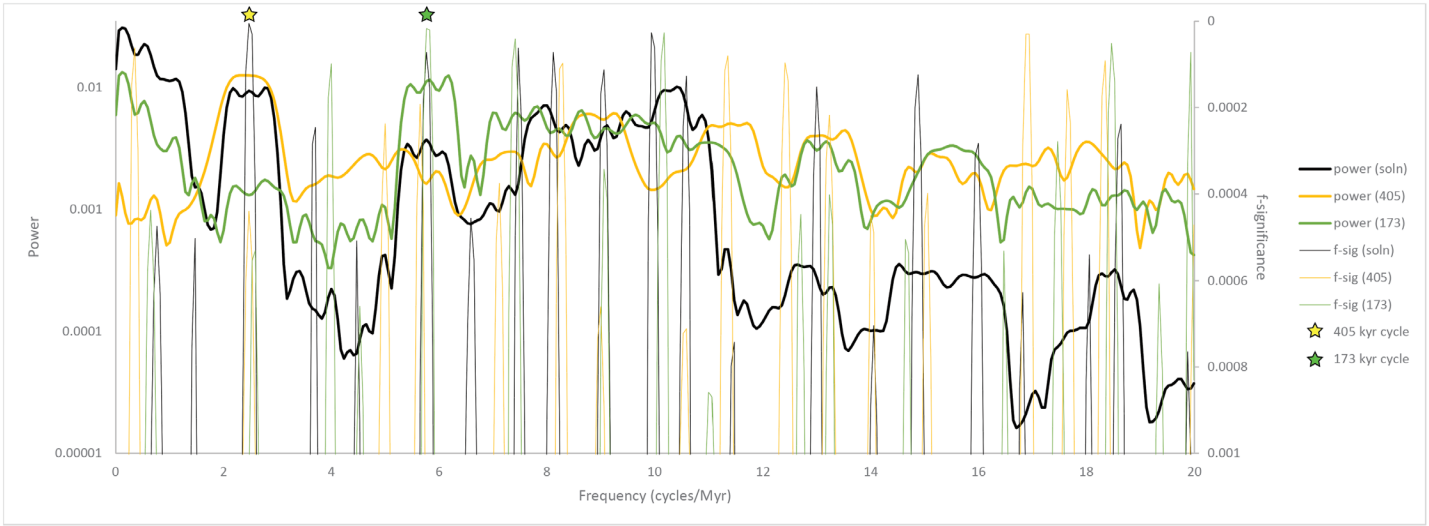

Figure 6. *Comparison of La2010d solution with equal parts eccentricity and inclination (blue), gamma ray data tuned to the 173 kyr cycle (gray), and gamma ray data tuned to the 405 kyr cycle (orange). Both new tunings use an age model based on gamma, and all MTM power spectra are at 2π bandwidth. Significant peaks showing overlap are labeled with period; red labels indicate two peaks with the same value. The 405 kyr and 173 kyr cycles are clearly expressed, as are other planetary cycles identified in Table 2.*

Published by EliScholar – A Digital Platform for Scholarly Publishing at Yale, 2021

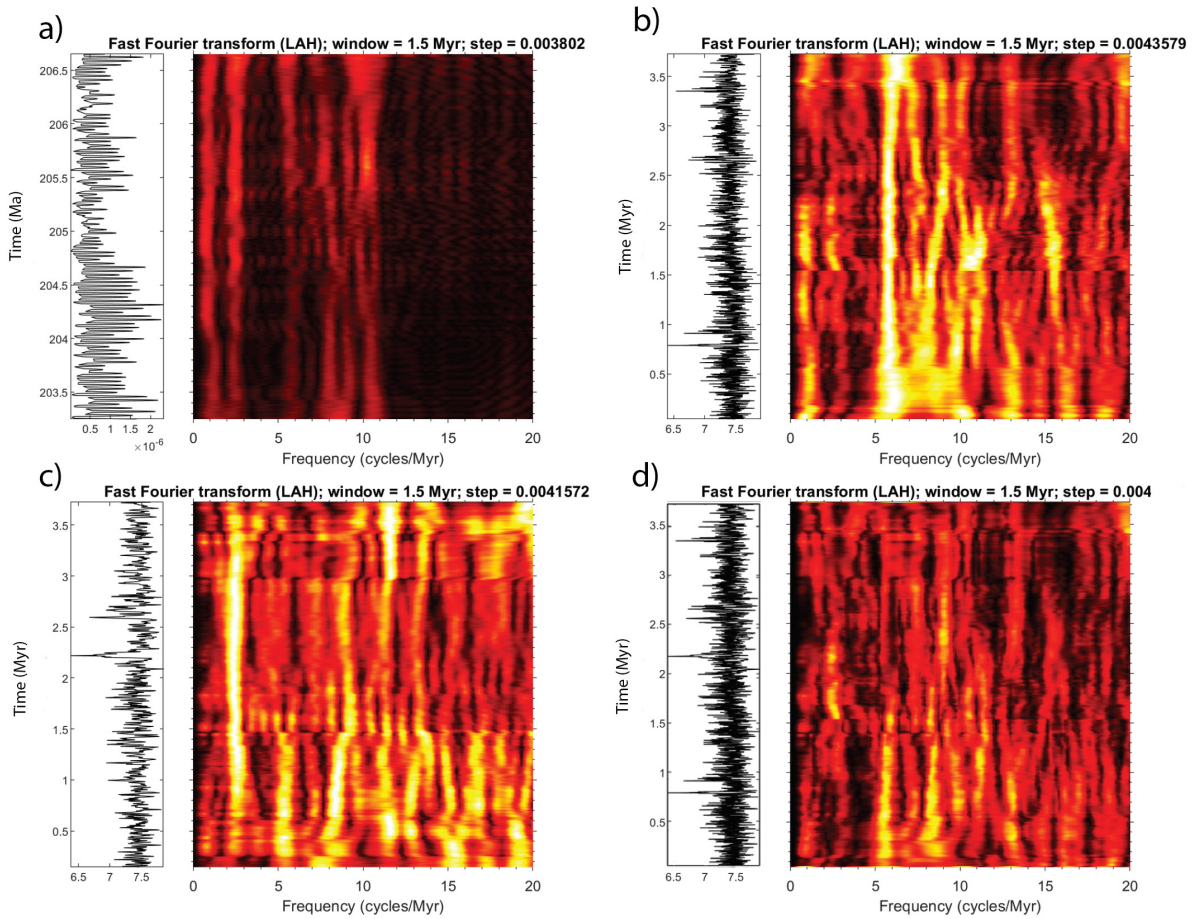

Figure 7. *Evolutionary power spectra of a) the La2010d solution with equal parts eccentricity and inclination, b) gamma ray data tuned to the 173 kyr cycle, c) gamma ray data tuned to the 405 kyr cycle, and d) both tunings multiplied together. A 1.5 Myr sliding window size was used for each spectrum. The 173 kyr cycle comes through most clearly in b and the 405 kyr cycle comes through most clearly in c, but the 405 kyr cycle and 1.5 Myr s3-s4 inclination cycle can be seen toward the left side of b, and the 173 kyr cycle can be seen at a frequency of ~5 in c. Both b and c show short eccentricity cycles in the 100 kyr range in the middle of the spectrum.*

inclination as well, calculated using values from Laskar (2020). In addition, we calculated high frequency cycles from low frequency cycles. In both cases, our results for the data tuned to the 173 kyr cycle and re-tuned to the 405 kyr cycle very closely matched those of the solution (Table 3).

DISCUSSION

Interval I, from 201.550–206.650 Ma, is qualitatively distinct from the others, with a characteristic low amplitude range in the depth rank and uniformly red mudstone composition, as opposed to the black of the other parts of the record. Low CO_2 in this interval may have caused overall tropical cyclicity to be muted, which in turn may have allowed the obliquity signal, having a larger theoretical effect at higher latitudes, to come through stronger than in other intervals. Relatedly, we were surprised to find that gamma radioactivity was the best proxy to represent this interval, as it is typically not as effective as others; this may also be a result of the homogeneity of the interval. Gamma ray data can thus be used as an objective proxy in sections with low amplitude data and red rock. Sonic velocity, while also objective, is less accurate especially in the low frequency range because it is sensitive to the diameter of the borehole; also, our sonic data changes qualitatively about halfway through the sequence and may be corrupted, although this would not affect Interval I.

We were able to identify and tune to both possible metronomes, the g2-g5 cycle and the s3-s6 cycle, with results that match the La2010d solution better than does the original tuning to a 405 kyr cycle based on a depth rank model. Yet we found that they did not match exactly: for example, the 405 kyr cycle appeared at a slightly higher frequency in the spectrum tuned to 173 kyr, and the 173 kyr cycle appeared at a slightly lower frequency in the spectrum tuned to 405 kyr. These complementary offsets in the eccentricity and inclination cycles of the different tunings are likely due to chaotic variation in the perihelion orbital precession of Venus and nodal precession of Earth (Jupiter and Saturn are assumed constant due to their mass). An optimized tuning based on our results could account for chaotic drift and provide a metronome not influenced by the variations of either planet, allowing us to accurately recover both s and g values. Iterative fitting of varying s3 and g2 values while keeping s6 and g5 constant and optimizing the match between all frequencies lacking these two fundamental secular frequencies after tuning with s3-s6 and g2-g5 might result in an independent way to recover s3 and g2. This would provide more stringent constraints for the astronomical solutions, allowing us to understand the actual evolution of the solar system from the Triassic to the present.

MTM period (kyr) tuned to 173 kyr		La2010d period (kyr)															
		s3-s4			s3-s6			s2-s4			s2-s3			s2-s6			
		1308.22			173.54			123.24			110.43			67.22			
s3-s4	1546.07				**200.08**	151.85	s4-s6	**136.06**	110.43	s2-s3	**120.61**	123.24	s2-s4	**70.86**	–	XXX	1308.22	s3-s4
s3-s6	173.54	**195.48**	150.50	s6-s4				**425.19**	–	XXX	**303.66**	67.22	s2-s6	**109.72**	110.43	s2-s3	173.54	s3-s6
s2-s4	122.35	**132.86**	110.43	s3-s2	**414.78**	–	XXX				**1062.40**	1308.22	s3-s4	**147.88**	151.85	s4-s6	123.24	s2-s4
s2-s3	110.43	**118.92**	122.35	s4-s2	**303.66**	68.30	s6-s2	**1133.48**	1546.07	s4-s3				**171.79**	173.54	s3-s6	110.43	s2-s3
s2-s6	68.30	**71.46**	–	XXX	**112.63**	110.43	s3-s2	**154.61**	150.50	s6-s4	**179.03**	173.54	s6-s3				67.22	s2-s6
			1546.07			173.54			122.35			110.43			68.30			
			s3-s4			s3-s6			s2-s4			s2-s3			s2-s6			

MTM period (kyr) tuned to 173 kyr

La2010d period (kyr)

Table 3. *Matrix designed by Olsen et al. (2019) as an internal check, showing inclination rather than eccentricity cycles. Long cycle periods calculated from short cycle periods, and vice versa (bold) are compared to observed periods (red) for both the La2010d solution (upper right) and the gamma ray data tuned to 173 kyr (lower left). Cells marked with XXX are combinations of cycles, not identified here.*

REFERENCES

Blackburn, T. J., Olsen, P. E., Bowring, S. A., McLean, N. M., Kent, D. V., Puffer, J., McHone, G., Rasbury, E. T., Et-Touhami, M., 2013, Zircon U-Pb geochronology links the end-Triassic extinction with the Central Atlantic Magmatic Province. *Science, 340*(6135), 941–945. https://doi.org/10.1126/science.1234204

Boulila, S., Vahlenkamp, M., De Vleeschouwer, D., Laskar, J., Yamamoto, Y., Pälike, H., Kirtland Turner, S., Sexton, P.E., Westerhold, T., & Rohl, U. (2018). Towards a robust and consistent middle Eocene astronomical timescale. *Earth and Planetary Science Letters, 486*, 94–107. https://doi.org/10.1016/j.epsl.2018.01.003

Hays, J. D., Imbrie, J., & Shackleton, N. J. (1976). Variations in the Earth's Orbit: Pacemaker of the Ice Ages. *Science, 194*(4270), 1121–1132. https://doi.org/10.1126/science.194.4270.1121

Hinnov, L. A. (2018). Cyclostratigraphy and Astrochronology in 2018. *Cyclostratigraphy and Astrochronology Stratigraphy & Timescales*, 1–80. https://doi.org/10.1016/bs.sats.2018.08.004

Kent, D.V., Olsen, P.E., Rasmussen, C., Lepre, C., Mundil, R., Irmis, R., Gehrels, G., Giesler, D., Geissman, J., & Parker, W. (2018). Empirical evidence for stability of the 405 kyr Jupiter-Venus eccentricity cycle over hundreds of millions of years. *Proceedings of the National Academy of Sciences, 115*(24), 6153–6158. https://doi.org/10.1073/pnas.1800891115

Laskar, J. (1999). The limits of Earth orbital calculations for geological time-scale use. *Philosophical Transactions of the Royal Society of London. Series A: Mathematical, Physical and Engineering Sciences, 357*(1757), 1735–1759. https://doi.org/10.1098/rsta.1999.0399

Laskar, J. (2020). Astrochronology. *Geologic Time Scale 2020*, 139–158. https://doi.org/10.1016/b978-0-12-824360-2.00004-8

Laskar, J., Fienga, A., Gastineau, M., & Manche, H. (2011). La2010: a new orbital solution for the long-term motion of the Earth. *Astronomy & Astrophysics, 532*. https://doi.org/10.1051/0004-6361/201116836

Laskar, J., Robutel, P., Joutel, J., Gastineau, M., Correia, A.C.M., & Levrard, B. (2004). A numerical solution for the insolation quantities of the Earth. *Astronomy & Astrophysics, 428*, 261–285. https://doi.org/10.1051/0004-6361:20041335

Li, M., Hinnov, L., & Kump, L. (2019). Acycle: Time-series analysis software for paleoclimate research and education. *Computers & Geosciences, 127*, 12–22. https://doi.org/10.1016/j.cageo.2019.02.011

Li, M., Huang, C., Hinnov, L., Ogg, J., Chen, Z. Q., & Zhang, Y. (2016). Obliquity-forced climate during the Early Triassic hothouse in China. *Geology, 44*(8), 623–626. https://doi.org/10.1130/g37970.1

Muller, R. A., & MacDonald, G. J. (2000). *Ice Ages and astronomical causes: data, spectral analysis and mechanisms.* Springer.

Olsen, P. E., & Kent, D. V. (1996). Milankovitch climate forcing in the tropics of Pangaea during the Late Triassic. Palaeogeography, *Palaeoclimatology, Palaeoecology, 122*(1–4), 1–26. https://doi.org/10.1016/0031-0182(95)00171-9

Olsen, P. E., Laskar, J., Kent, D. V., Kinney, S. T., Reynolds, D. J., Sha, J., & Whiteside, J. H. (2019). Mapping Solar System chaos with the Geological Orrery. *Proceedings of the National Academy of Sciences, 116*(22), 10664–10673. https://doi.org/10.1073/pnas.1813901116

Park, J., Lindberg, C. R., & Vernon, F. L. (1987). Multitaper spectral analysis of high-frequency seismograms. *Journal of Geophysical Research, 92*(B12), 12675. https://doi.org/10.1029/JB092iB12p12675

Rasmussen, C., Mundil, R., Irmis, R. B., Geisler, D., Gehrels, G. E., Olsen, P. E., Kent, D.V., Lepre, C., Kinney, S. T., Geissman, J. W., Parker, W. G. (2020). U-Pb zircon geochronology and depositional age models for the Upper Triassic Chinle Formation (Petrified Forest National Park, Arizona, USA): Implications for Late Triassic paleoecological and paleoenvironmental change. *GSA Bulletin*. https://doi.org/10.1130/b35485.1

Storm, M. S., Hesselbo, S. P., Jenkyns, H. C., Ruhl, M., Ullmann, C. V., Xu, W., Leng, M. J., Riding, J. B., & Gorbanenko, O. (2020). Orbital pacing and secular evolution of the Early Jurassic carbon cycle. *Proceedings of the National Academy of Sciences, 117*(8), 3974–3982. https://doi.org/10.1073/pnas.1912094117

Thomson, D. J. (1982). Spectrum estimation and harmonic analysis. *Proceedings of the IEEE, 70*(9), 1055–1096. https://doi.org/10.1109/PROC.1982.12433

Whiteside, J. H., Grogan, D. S., Olsen, P. E., & Kent, D. V. (2011a). Climatically driven biogeographic provinces of Late Triassic tropical Pangea. *Proceedings of the National Academy of Sciences, 108*(22), 8972–8977. https://doi.org/10.1073/pnas.1102473108

Whiteside, J. H., Olsen, P. E., Eglinton, T. I., Cornet, B., McDonald, N. G., & Huber, P. (2011b). Pangean great lake paleoecology on the cusp of the end-Triassic extinction. Palaeogeography, *Palaeoclimatology, Palaeoecology, 301*(1–4), 1–17. https://doi.org/10.1016/j.palaeo.2010.11.025

Published by EliScholar – A Digital Platform for Scholarly Publishing at Yale, 2021